Unidirectional DC/DC Modular Multilevel Converter for Offshore Windfarm with the Control Strategy Based on Stationary Frame

He Liu*, Mohamed Dahidah*, R. T. Naayagi*, Matthew Armstrong*, and James Yu†

**School of electrical electronic engineering, newcastle university, newcastle upon tyne, NE1 7RU, UK*
(Email:h.liu3@newcastle.ac.uk)
†S.P. Energy Networks, Blantyre, UK
(Email:Yu@scottishpower.com)

Keywords: Modular multilevel converter, DC/DC converter, DC collection point, off-shore windfarm, generalized stationary frame regulators.

Abstract

This paper presents the design and control of an advanced unidirectional DC/DC Modular Multilevel Converter (MMC) that facilitate the integration of off-shore windfarms with the High-Voltage Direct Current (HVDC) transmission system. The proposed converter deploys a single-phase MMC inverter coupled with series-connected rectifier modules through multiple medium frequency transformers. Unlike the conventional d-q control method, which involves multiple transformations, this paper also proposes a simple control strategy that directly act on the ac output of the MMC, under the stationary reference frame.

1 Introduction

High voltage direct current (HVDC) transmission system is a well-established and proven technology for delivering large-scale energy over a long distance with less power losses and lower reactive power requirements [1]. Large-scale offshore wind energy is increasingly growing and the interconnection between multiple farms becomes more challenging. Medium-voltage DC collection networks are a promising technology for such integration aiming to eliminate the extra conversion stages and improve the system reliability [2]. High-voltage high-power DC/DC converters, are the key enabler for the dc grid. Various converter topologies have been investigated and reported in the literature, which can be broadly classified as combined (consisting of multiple converter modules) and modular multilevel topologies [3].

Most notably, Dual Active Bridge (DAB) converter has received a great attention from the research community due to its distinctive features, such as: galvanic isolation, bidirectional power flow and ability to operate with high switching frequency [4]. However, the high-voltage and high-power requirements for the DC/DC converter based HVDC systems, necessitate series and/or parallel combinations at both, the power semiconductor devices and converter modules levels [5]. Furthermore, as the requirement for offshore DC collection point is to deliver a high-voltage, facilitating the connection with HVDC transmission system, the input parallel output series (IPOS) configuration is commonly preferred [6], which is retained for this work as well. There are several papers investigated IPOS combined converter as DC collection point for the HVDC system [7-11]. However, for such a converter, the full soft switching operation can only be achieved with a limited load and input voltage range, which substantially limits the efficiency and the performance of the converter due to the increased switching losses and electromagnetic interference [8].To address this problem, an external large resonant inductor is usually connected in series with the transformer to extend the soft switching range, but the large inductance has a detrimental effect on the performance of the converter since it results in increased duty cycle losses, as well as a severe voltage ringing due to the resonance between the inductance and the junction capacitance in the converter [9]. The concept of using a saturation inductor instead of linear inductor has been discussed in [11], which effectively extends the soft switching range with lower conduction losses and without a significant duty cycle loss. However, a large core is required for thermal dissipation, limiting the whole system power density and large-scale applications.

The research in this paper alleviates the abovementioned issues by proposing a modular DC/DC converter, employing MMC at the primary side of a medium frequency transformer. The DC voltage is collected at the secondary side through series-connected diode-bridge rectifier modules. The proposed system is highly modular and considerably reduces the switching losses. An enhanced control method is also proposed to control the operation of the converter.

The rest of the paper is organized as follows: Section II describes the circuit configuration of the proposed DC/DC converter and its operating principle. The analysis of power balance of MMC at the primary side is presented in Section III. A simple control strategy based on the stationary reference frame is derived in Section IV. Section V illustrates simulation results. Finally, the work is concluded in Section VI.

2 Proposed DC/DC converter based system

Fig.1 shows a simplified schematic diagram of the proposed converter which can be functioned as DC collection point, where a single-phase (two-leg) MMC inverter producing a controllable AC voltage is connected at the primary side of multiple medium frequency (400Hz) transformers. The DC output voltage is obtained through series-connected full-bridge rectifier modules at the multi-winding secondary side of the transformers. It is worth noting that the design is fully modular at both sides and can be easily expanded as required by simply adding more modules.

3 The mathematical model of the proposed converter

Fig. 2 shows the equivalent circuit of one-leg (phase A) of the MMC, where V_{dc_in} and I_{dc_in} are the converter's DC input voltage and current, respectively. V_{ap} and V_{aN} are the upper and lower arm voltages of the cascede submodules of Phase A leg, respectively. I_{aP} and I_{aN} are the current of the upper and lower arms, respectively. E_a is the equivalent output phase voltage as shown in Fig.2(b) and V_a is output AC voltage, respectively. I_{cir} and I_a are circulating current and ouput AC current, respectively.

From Fig.2, the upper and lower arm currents of Phase A leg can be expressed as:

$$I_{aP} = I_a/2 + I_{cir} \quad (1)$$

$$I_{aN} = -I_a/2 + I_{cir} \quad (2)$$

where the circulating current, I_{cir} is flowing through both the upper and lower amrs.

It should be noted that the circulating current has no effect on the ouptut phase current and can be expressed as:

$$I_{cir} = (I_{aP} + I_{aN})/2 \quad (3)$$

With reference to (1) and (2), the equation of output AC current I_a can be expressed in terms of upper and lower arm currents as:

$$I_a = I_{aP} - I_{aN} \quad (4)$$

Considering *n* as the neutral point, applying the Kirchhoff Voltage Laws (KVL) for the schematic diagram of one-lge MMC as shown in Fig.2(a) , therefore, the upper and lower voltages can be derived as:

$$V_{aP} = \frac{V_{dc}}{2} - V_a - L_{arm}\frac{dI_{aP}}{dt} \quad (5)$$

$$V_{aN} = \frac{V_{dc}}{2} + V_a - L_{arm}\frac{dI_{aN}}{dt} \quad (6)$$

Combining (5) and (6), the output phase voltage V_a can be expressed as:

$$V_a = \frac{1}{2}(V_{aN} - V_{aP}) - \frac{1}{2}L_{arm}\frac{d(I_{aN}-I_{aP})}{dt} \quad (7)$$

Substituting (4) into (7), the equivalent output phase voltage E_a can be given by:

$$E_a = \frac{1}{2}(V_{aN} - V_{aP}) = V_a + \frac{1}{2}L_{arm}\frac{dI_a}{dt} \quad (8)$$

Therefore, the mathmatical model of the one-leg MMC can be derived by rearranging (8) as:

$$\frac{1}{2}L_{arm}\frac{dI_a}{dt} = E_a - V_a \quad (9)$$

According to (9), the equivalent circuit of Phase A can be expressed as Fig.2 (b).

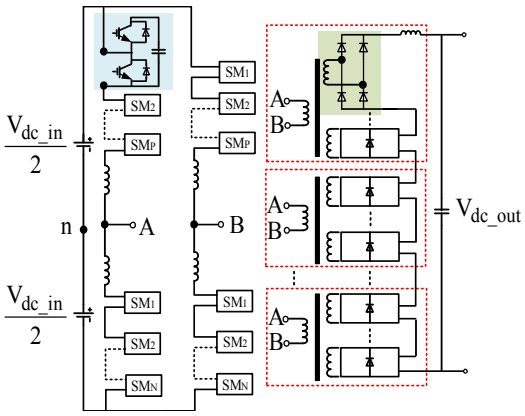

Fig.1. Typical schematic diagram of off-shore HVDC transmission system using the proposed DC/DC converter functioned as DC collection point

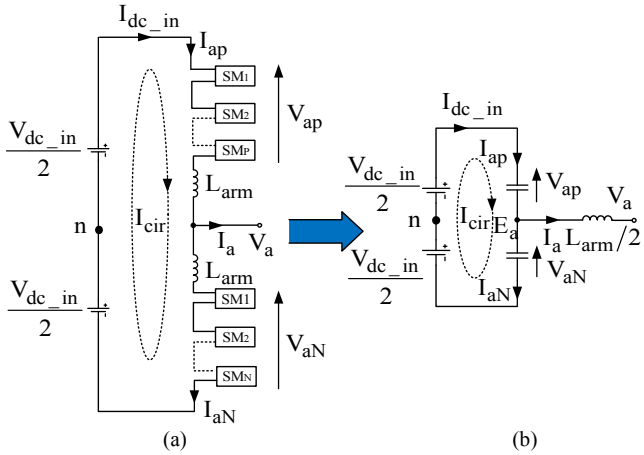

Fig.2. (a) Schematic diagram of the one-leg MMC and (b) its equivalent circuit

Similarly, the mathmatical model of the second leg of MMC (i.e. phase B), can be given by:

$$\frac{1}{2}L_{arm}\frac{dI_b}{dt} = E_b - V_b \quad (10)$$

where E_b and V_b are the equivalent output pahse voltage and output AC voltage of Phase B, respectively and I_b is the ouptut AC current of Phase B.

Combining (9) and (10), the mathmatical model of single pahse (two-leg) MMC can be expressed as:

$$\frac{1}{2}L_{arm}\frac{dI_a}{dt} - \frac{1}{2}L_{arm}\frac{dI_b}{dt} = (E_a - E_b) - (V_a - V_b) \quad (11)$$

For simplicity, let:

$$V_{Po} = E_a - E_b \quad (12)$$

$$V_{ab} = V_a - V_b \quad (13)$$

Hence, (11) can be re-written as:

$$\frac{1}{2}L_{arm}\frac{d(I_a-I_b)}{dt} = V_{Po} - V_{ab} \quad (14)$$

For a single phase (two-leg) MMC, the relationship between the output current of phase A and B can be expressed as :

$$I_P = I_a = -I_b \quad (15)$$

where I_P is the transformer primary current of the proposed converter.

Substituting (15) into (14), yields:

$$L_{arm}\frac{dI_P}{dt} = V_{Po} - V_{ab} \quad (16)$$

where the V_{Po} and V_{ab} can be considered as the equivalent primary voltage and primary terminal voltage of the transformer, respectively. I_P is transformer primary voltage. L_{arm} is arm inductance.

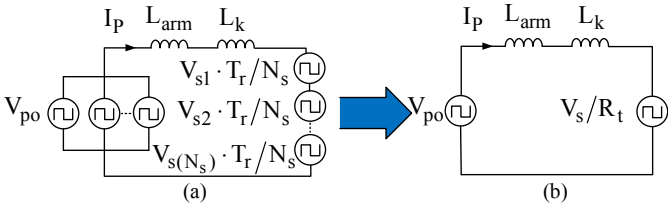

Fig.3. (a) The equivalent circuit of the proposed converter referred to primary side (b) and its simplifiy equivalent circuit

From Fig.1, the primary side of the transformers are connected in parallel, which are equivalent to a parallel connection of voltage sources (V_{Po}). Similarly, the secondary side of the transformer is made of a combination of individual and isolated modules. This can be regarded as a series connection of voltage sources ($V_{s1}, V_{s2}, \dots, V_{s(N_s)}$). Therefore, the total equivalent voltage at the secondary side of the transformer V_s, can be expressed as:

$$V_s = V_{s1} + V_{s2} + \cdots + V_{s(N_s)} \quad (17)$$

where N_s is the number of rectifier modules at the secondary. If the equivelant primary-to-secondary winding turns ratio is R_t and the turns ratio of primary to each individual secondary winding is T_r, the equivelant secondary volatge V_s when it is referred to the primary side can then be given by:

$$V_{ab} = V_s R_t = V_{s1}\frac{T_r}{N_s} + V_{s2}\frac{T_r}{N_s} + \cdots + V_{s(N_s)}\frac{T_r}{N_s} \quad (18)$$

Substituting (16) into (18), and with the transformer's leakage inductance L_k referred to the primary side, the primary referred equivalent circuit of the proposed converter converter can be expressed by (19) and schematically represented by Fig.3.

$$(L_{arm} + L_k)\frac{dI_p}{dt} = V_{Po} - V_s R_t \quad (19)$$

3 Power transfer characteristics of the proposed converter

3.1 Voltage and current Key-waveforms of the proposed converter

To simplify the analysis and to facilitate easy understanding, the following assumptions are considered for the output voltage waveform of the MMC. 1) The submodule capacitor voltages are well balanced and ripple-free. 2) The converter is operating with a unity modulation index. 3) With high number of submodules, resulting in small steps in the output waveform, which then can be approximated as trapezoidal waveform as illustrated in Fig.4. It is worth noting also that, in this work, the well-known carrier-phase-shift pulse width modulation (CPS-PWM) technique is applied. The detailed analysis and the principle of operation of CPS-PWM have been well documented and readily available from [12], therefore, no further details will be presented in this paper.

Fig.4 shows typical voltage of primary-referred equivalent circuit of the proposed converter, where the power is always transferred from V_{dc_in} to V_{dc_out}(i.e. unidirectional). It should be noted that θ_{stair} in Fig.4 is the interval of the voltage rising or falling transition of the V_{Po}, V_s is the secondary equivalent voltage which is equal to the sum of $V_{s1} + V_{s2} + \ldots + V_{s(Ns)}$ and

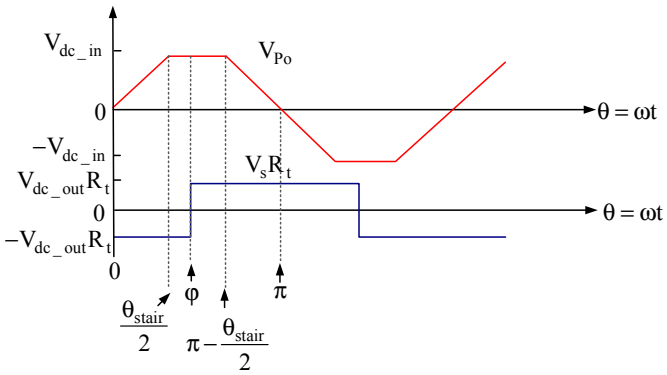

Fig.4. Typical voltage of primary-referred equivalent circuit of the proposed converter.

φ is the phase shift angle by which V_s lags V_{Po}.

3.2 Derivation of the proposed converter's output power

It should be noted that in the succeeding analysis, the following assumptions are considered: 1) owing to the waveform symmetry, only half-cycle of the AC output waveform is considered as shown in Fig.4. 2) for simplicity, the peak value of V_{Po} and V_s are equal to V_{dc_in}, and V_{dc_out}, respectively, (i.e. ignoring any voltage drop across the circuit components). According to the Fig.4, the output power can be derived in the following operational intervals:

Interval 1 *($0 \le \theta < \theta_{stair}/2$)*:
As it can be noticed from Fig.4, during this interval$V_s(\theta)$ is equal to the $-V_{dc\_out}$, and its primary refered voltage is $V_{dc\_out}R_t$. Therefore, $V_{po}(\theta)$ and $I_p(\theta)$ can be expressed as:

$$V_{po}(\theta) = \frac{2V_{dc\_in}}{\theta_{stair}}\theta \quad (20)$$

$$I_p(\theta) = I_p(0) + \frac{1}{L}\int_0^{\theta}\left[V_{po}(\theta) - R_t V_s(\theta)\right]d\theta \quad (21)$$

replacing $V_s(\theta)$ by $-V_{dc\_out}$ and substituting (20) into (21), yields:

$$I_p(\theta) = I_p(0) + \frac{1}{L}\left[\frac{V_{dc\_in}}{\theta_{stair}}\theta^2 + V_{dc\_out}R_t\theta\right] \quad (22)$$

According to (22), at $\theta = \frac{\theta_{stair}}{2}$, one can get:

$$I_p\left(\frac{\theta_{stair}}{2}\right) = I_p(0) + \frac{\theta_{stair}}{2L}\left(\frac{V_{dc\_in}}{2} + V_{dc\_out}R_t\right) \quad (23)$$

According to (20) and (22), the output energy during this interval can be obtained by:

$$\mathrm{E}_1 = \int_0^{\frac{\theta_{stair}}{2}} V_s(\theta) * I_p(\theta)d\theta = -\frac{V_{dc\_out}\cdot\theta_{stiar}(3V_{dc\_out}\theta_{stair}R_t^2 + R_t V_{dc\_in}\theta_{stiar} + 12LR_t I_p(0))}{24\cdot L} \quad (24)$$

Interval 2 *($\theta_{stair}/2 \le \theta < \varphi$)*:
During this interal, $V_s(\theta)$ remains as $-V_{dc\_out}$, $V_{po}(\theta)$ is equal to the V_{dc_in}, and $I_p(\theta)$ can be expressed as:

$$I_p(\theta) = I_p\left(\frac{\theta_{stair}}{2}\right) + \frac{1}{L}\left[V_{po}(\theta) - R_t V_s(\theta)\right]\left(\theta - \frac{\theta_{stair}}{2}\right) \quad (25)$$

Substituting $V_s(\theta) = -V_{dc\_out}$,$V_{po}(\theta) = V_{dc\_in}$ and (25) into $I_p(\theta)$ yields,

$$I_p(\theta) = I_p(0) + \frac{1}{L}\left[\left(V_{dc\_in} + V_{dc\_out}R_t\right)\theta - \frac{V_{dc\_in}\theta_{stair}}{4}\right] \quad (26)$$

From (26), at $\theta = \varphi$, one can get:

$$I_p(\varphi) = I_p(0) + \frac{1}{L}\left[\left(V_{dc\_in} + V_{dc\_out}R_t\right)\varphi - \frac{V_{dc\_in}\theta_{stair}}{4}\right] \quad (27)$$

Similarly, the transferred energy during this interval is given by:

$$E_2 = \int_{\frac{\theta_{stair}}{2}}^{\varphi} V_s(\theta) * I_p(\theta) d\theta = \frac{V_{dc\_out}(\theta_{stair}-2\varphi)(V_{dc\_out}\theta_{stair}R_t^2+2V_{dc\_out}\varphi R_t^2+2R_tV_{dc\_in}\varphi+4LR_tI_p(0))}{8L} \quad (28)$$

Interval 3 *($\varphi \le \theta < \pi - \frac{\theta_{stair}}{2}$)*:

During this interval, $V_s(\theta)$ is equal to V_{dc_out}, $V_{po}(\theta)$ remains as V_{dc_in}, and $I_p(\theta)$ can be expressed as:

$$I_p(\theta) = I_p(\varphi) + \frac{1}{L}\left[V_{po}(\theta) - R_tV_s(\theta)\right](\theta - \varphi) \quad (29)$$

Substituting $V_s(\theta) = V_{dc\_out}$,$V_{po}(\theta) = V_{dc\_in}$ and (27) into (29) yields,

$$I_p(\theta) = I_p(0) + \frac{1}{L}\left[(V_{dc\_in} - V_{dc_{out}}R_t)\theta + 2V_{dc_{out}}R_t\varphi - \frac{V_{dc\_in}\theta_{stair}}{4}\right] \quad (30)$$

From (30), at $\theta = \pi - \frac{\theta_{stair}}{2}$, one can get:

$$I_p\left(\pi - \frac{\theta_{stair}}{2}\right) = I_p(0) + \frac{1}{L}\left[(V_{dc\_in} - V_{dc\_out}R_t)\left(\pi - \frac{\theta_{stair}}{2}\right) + 2V_{dc\_out}R_t\varphi - \frac{V_{dc\_in}\theta_{stair}}{4}\right] \quad (31)$$

Similarly, the output energy during this interval can be expressed as:

$$E_3 = \int_{\varphi}^{\pi-\frac{\theta_{stair}}{2}} V_s(\theta) * I_p(\theta) d\theta = -\frac{1}{8L}V_{dc_{out}}(\theta_{stair} - 2\pi + 2\varphi)(V_{dc_{out}}\theta_{stair}R_t^2 - 2\pi V_{dc_{out}}R_t^2 + 6V_{dc\_out}\varphi R_t^2 - 2R_t.V_{dc_{in}}\theta_{stair} + 2R_tV_{dc\_in}\varphi + 4LR_tI_p(0) + 2R_t\pi V_{dc\_in}) \quad (32)$$

Interval 4 *($\pi - \frac{\theta_{stair}}{2} \le \theta < \pi$)*:

During this interval, $V_s(\theta)$ remains as V_{dc_out}. The primary voltage, $V_{po}(\theta)$ and the primary current, $I_p(\theta)$ can be expressed as:

$$V_{po}(\theta) = \frac{V_{dc\_in}}{\theta_{stair}}(2\theta - 2\pi) \quad (33)$$

$$I_p(\theta) = I_p\left(\pi - \frac{\theta_{stair}}{2}\right) + \frac{1}{L}\int_{\pi-\frac{\theta_{stair}}{2}}^{\theta}\left[V_{po}(\theta) - R_tV_s(\theta)\right]d\theta \quad (34)$$

Substituting $V_s(\theta) = V_{dc\_out}$, (30) and (33) into (34) yields:

$$I_p(\theta) = I_p(0) - \frac{1}{L}\left[\frac{V_{dc\_in}}{\theta_{stair}}\theta^2 + \frac{V_{dc\_out}.\theta_{stair}R_t - 2\pi V_{dc\_in}}{\theta_{stair}}\theta - \frac{4V_{dc\_out}\theta_{stair}R_t - 2\pi^2V_{dc\_in} - V_{dc\_in}\theta_{stair}^2 + 2\pi V_{dc\_in}\theta_{stair}}{2\theta_{stair}}\right] \quad (35)$$

From (35), with $\theta = \pi$, one can write the primary current as:

$$I_p(\pi) = I_p(0) + \frac{1}{L}\left(\pi V_{dc\_in} - 2V_{dc_{out}}\varphi R_t - \pi V_{dc_{out}}R_t - \frac{V_{dc\_in}\theta_{stair}}{2}\right) \quad (36)$$

Hence, from (33) and (35), the output energy during this interval can be obtained by (37) below.

$$E_4 = \int_{\pi-\frac{\theta_{stair}}{2}}^{\pi} V_s(\theta) * I_p(\theta) = \frac{1}{24L}V_{dc_{out}}\vartheta_{stair}(3V_{dc_{out}}\theta_{stair}R_t^2 - 12\pi V_{dc_{out}}R_t^2 + 24V_{dc_{out}}\varphi R_t^2 - 7R_tV_{dc_{in}}\theta_{stair} + 12LR_tI_p(0) + 12R_t\pi V_{dc\_in}) \quad (37)$$

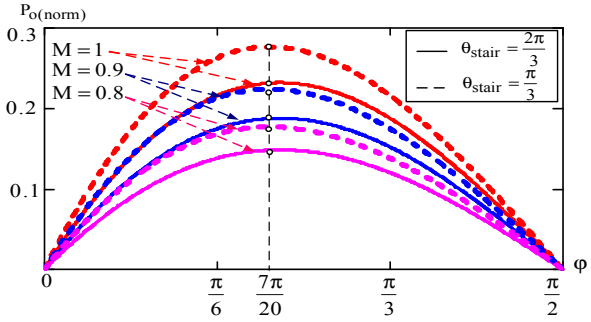

Fig.5. Normalized output power versus pahse shift angle φ of the proposed converter.

Therefore, from (24), (28), (32), and (37), the ouput power of the proposed converter can be calcultaed as:

$$P_{out} = \frac{E_1+E_2+E_3+E_4}{\pi} \quad (38)$$

Due to half-cycle symmetry, $I_p(0) = -I_p(\pi)$. Therefore, according to (36), the intial current $I_p(0)$ can be calculated as:

$$I_p(0) = \frac{2\pi V_{dc_{out}}R_t - 4V_{dc_{out}}\varphi R_t + V_{dc\_in}\theta_{stair} - 2\pi V_{dc\_in}}{4L} \quad (39)$$

Letting $G = \frac{V_{dc_{out}}R_t}{V_{dc\_in}}$ in (38) and (39), the ouput power of the proposed converter at any phase shift angle, φ, can be expressed by:

$$P_{out}(\varphi) = -\frac{GV_{dc\_in}^2(\theta_{stair}^2 + 12\varphi^2 - 12\pi\varphi)}{12\pi L} \quad (40)$$

where G is defined with the primary-referred dc voltage gain of the proposed converter, often referred to as the DC conversion ratio.

3.3 Analysis of the proposed converter's output power

Similar to the conventional Single Active Bridge (SAB) DC/DC converter [13], based on the different phase shift angle φ, the proposed converter has two operating modes, 1) $0 \le \varphi < \frac{\theta_{stair}}{2}$, and 2) $\frac{\theta_{stair}}{2} \le \varphi < \frac{\pi}{2}$. Therefore, the corresponding I_P in the different modes can also be obtained. Then, the ouput power in the different modes can be derived as :

$$P_{o(norm)} = \begin{cases} -\frac{M^2\varphi(3\theta_{stair}^2 - 6\pi\theta_{stair} + 4\varphi^2)}{\theta_{stair}} & (0 \le \varphi < \frac{\theta_{stair}}{2}) \\ -\frac{M^2(\theta_{stair}^2 + 12\varphi^2 - 12\pi\varphi)}{2} & (\frac{\theta_{stair}}{2} \le \varphi < \frac{\pi}{2}) \end{cases} \quad (41)$$

Where modulation index $M \in [0,1]$ is introduced in oder to get the generalized equation of the ouput power.

Fig. 5 illustrates the variation of the normalized power of (41) with respect to phase shift angle φ. It is clear that the power transfer capability of the proposed converter is influnced by the modualation index M, θ_{stair}, and the phase shift angle φ, where the highest power is achieved when the modulation index is unity. on the other hand, increasing θ_{stair}, decreases the power transfer capability of the proposed converter.

4 Control strategy of the proposed converter

Considering one-leg MMC as an example, the implementation of the proposed closed-loop control is

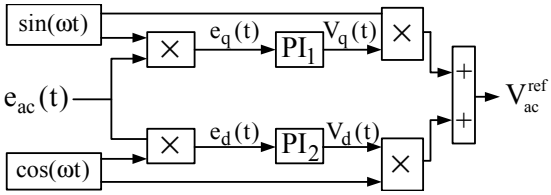

Fig.6. Block diagram of implementation of the close loop control.

illustrated in Fig.6. It is realized by multiplying the transfer functions of the conventional Proportional Integral (PI_1 and PI_2) regulators with the sin and cos reference signals [30]. Equation (42) describes the implementation of the proposed control method, which is schematically depicted in Fig.6.

$$V_{ac}^{ref}(\mathrm{t}) = \{[e_{ac}(t)\cdot \sin(\omega \mathrm{t})] * h_{dc}(t)\}\cdot \sin(\omega t) + \{[e_{ac}(t)\cdot \cos(\omega \mathrm{t})] * h_{dc}(t)\}\cdot \cos(\omega t) \quad (42)$$

where $e_{ac}(t)$ is the input AC error signal, $h_{dc}(t)$ represents the unit impulse response under time domain of PI regulator, and $*$ ' donates the convolution product. The output of this control loop $V_{ac}^{ref}(t)$ is used as a modulating signal to drive the power switches of phase A.

Actually, after multiplying with reference signal, sine and cos, the error signal $e_{ac}(t)$ is converted into a DC and AC components with two times the fundamental frequency. This is then fed into the PI regulators, which perform the integration to get the steady-state error and also work as a low-pass filter to extract out the DC signal to achieve a zero steady-state error in the stationary reference frame. Applying Laplace transform to (43), yields

$$V_{ac}^{ref}(s) = \frac{1}{2}[H_{dc}(s+j\omega) + H_{dc}(s-j\omega)]e_{ac}(s) \quad (43)$$

For a conventional PI regulator, the Laplace transform of a unity impulse response can be described by the following equation:

$$H_{dc}(s) = k_p + \frac{k_i}{s} \quad (44)$$

By substituting (66) into (65), the transfer function of the control system with derived generalized integrator can be given as:

$$V_{ac}^{ref}(s) = (k_p + \frac{k_i \cdot s}{s^2+\omega^2})e_{ac}(s) \quad (45)$$

where k_p is the proportional constant which is used to improve the transient response of the control system, k_i is the integral constant and ω is the resonant frequency of the derived integrator. Therefore, the infinity gain can be achieved when s = jω

5 Simulation results

A simulation model of the proposed converter rated at 80 MW/200kV is developed with the tabulated parameters in table I using MATLAB/SIMULINK to validate the feasibility and the effectiveness of the proposed system and its control performance. In this paper, the MMC is constructed with fifteen half-bridge SM per arm and there are two series-connected diode-bridge rectifiers at the secondary side of the transformer. Furthermore, the medium frequency transformer with turn ratios of 2:3:3 is chosen, however different turns ratio can be simply considered for different stepping gain.

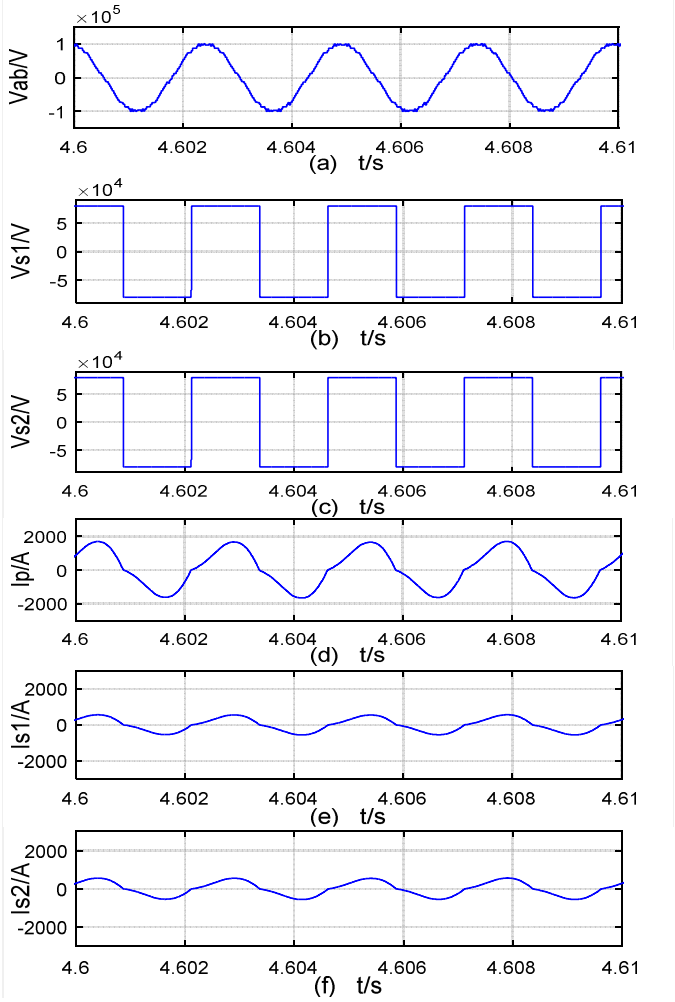

Fig.7. (a) Transformer primary terminal voltage waveform V_{ab}(b) transformer secondary winding-one voltage waveform V_{s1}. (c) transformer secondary winding-two voltage waveform V_{s2}. (d) transformer primary current waveform I_p. (e) transformer secondary winding-one current waveform I_{s1}(f) transformer secondary winding-two current waveform I_{s2}.

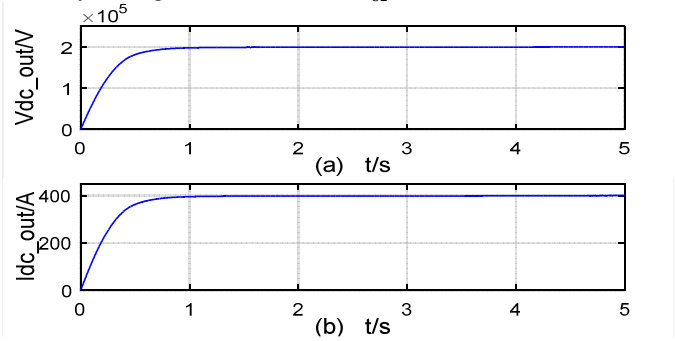

Fig.8. The output waveforms of the Proposed converter under steady-state operation. (a) output DC voltage (b) output DC current.

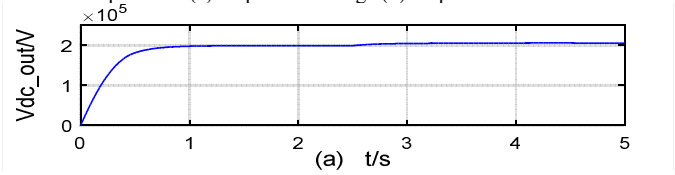

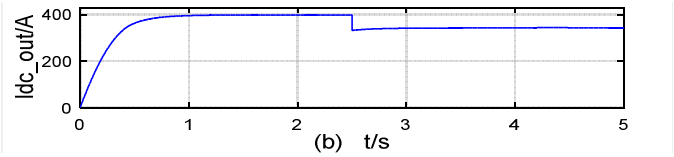

Fig.9. The output waveforms of the Proposed converter under a step change at 2.5s (a) output DC voltage. (b) output DC current.

The steady-state voltage and current of the proposed converter, operating at 400Hz is depicted in Fig.7.

The output DC voltage of the proposed converter is shown in Fig.8 and with the given transformer turns ratio in this paper (i.e. $W_p : W_{s1} : W_{s2} = 2:3:3$, where W_p, W_{s1}, and W_{s2} are the primary winding, the corresponding secondary winding-one and winding-two, respectively), the average output DC voltage is maintained around 200kV.

The performance of the proposed control strategy is further investigated and confirmed with a step change in the output load ((i.e. 500Ω to 600Ω). Fig.9 shows the dynamic response of the controller when the load changed at $t = 2.5s$, causing the output current I_{dc2} to decrease from 400A to 333A, however the output voltage is perfectly maintained constant, which confirms the effectiveness of the proposed control system.

PARAMETER	Value
Rated power	80MW
Input DC voltage	100kV
Output DC voltage	200kV
Submodule numbers of MMC per arm	15
Submodule numbers of combined converter	2
Transformer ratio	2:3:3
Submodule capacitor of MMC	2.2mF
Inductance of per arm	1mH
Output capacitor	3mF
Output inductor	1mF
Switching frequency	2000Hz
AC fundamental frequency	400Hz

Table I: Parameters of the simulation

6 Conclusion

A modular unidirectional dc/dc converter based DC collection point is presented in this paper. The proposed converter utilized the state-of-the-art MMC at the primary side of a medium frequency transformer and cascaded diode-bridge rectifier modules at the secondary side. The converter design features modularity, expandability, redundancy, galvanic isolation, and lower voltage and current stress on power devices. Detailed design analysis is presented and the parameters that effect the operation of the converter are defined and thoroughly discussed. The presented control strategy abolishes all complexity associated with the transformation and inverse transformation required for the conventional *d-q* synchronous reference frame methods. The derived generalized controller directly acts on the AC single of the primary side, avoiding complex transformation and providing robustness against system variations. The performance of the proposed converter and its control strategy is validated through various simulation results.

References

[1] P.Bresesti, W.L.Kling, R.L.Hendriks, R.Vailati, "HVDC Connection of Offshore Wind Farms to the Transmission System," *IEEE Trans. Energy Convers.,* vol.22, no.1, pp.37-43, Mar.2007.

[2] J.Robinson, D.Jovcic, G.Joos, "Analysis and Design of an Offshore Wind Farm Using a MV DC Grid," *IEEE Trans. Power Del.,* vol.25, no.4, pp.2164-2173, Oct. 2010.

[3] C. Sun, J. Zhang, X. Cai, and G. Shi, "Voltage Balancing Control of Isolated Modular Multilevel dc-dc Converter for Use in dc Grids with Zero Voltage Switching," *IET Power Electron.,* vol. 9, no. 2, Feb. 2016.

[4] J. Everts, "Closed-Form Solution for Efficient ZVS Modulation of DAB Converters," *IEEE Trans. Power Electron.,* vol.32, no.10, pp.7561-7576, Oct. 2017.

[5] W. Chen, X. Ruan, H. Yan, and C. Tse, "DC/DC Conversion System Consisting of Multiple Converter Modules: Stability, Control, and Experimental Verifications," *IEEE Trans. Power Electron.*, vol.24, no.6, Jun. 2009.

[6] T. Li, and L. Parsa, "Design, Control and Analysis of a Fault Tolerant Soft-Switching DC-DC Converter for High Power High Voltage Applications," *IEEE Trans. Power Electron.,* no.99, Mar. 2017.

[7] J.Adhikari, A.K.Rathore, S.Kumar Panda, "Modular Interleaved Soft-Switching DC-DC Converter for High-Altitude Wind Energy Application," *IEEE Trans. Emerging and Selected Topics Power Electro.,* vol.2, no.4, pp.727-738, Dec.2014.

[8] R.A.Friedemann, F.Krismer, J.W.Kolar, "Design of a minimum weight dual active bridge converter for an Airborne Wind Turbine system," in *Proc. IEEE Appl. Power Electron. Conf. Expo.,* 2012, pp.509-316.

[9] A. Chub, O. Husev, and D. Vinnikov, "Input-parallel output-series connection of isolated quasi-Z-source DC-DC converters," in *Proc. Electron. Power Quality Supply Rel. Conf.,* 2014, pp.277–284.

[10] C. Song, R. Zhao, W. Lin, Z. Zeng, "A novel control strategy for input-parallel-output-series inverter system," in *Proc. Int. Conf. Electric. Machines systems,* 2011.

[11] G. Hua, F. C. Lee, M. M. Jovanovic, "An improved full-bridge zero-voltage-switched PWM converter using a saturable inductor," *IEEE Trans. Power Electron.,* vol.8, no.4, pp.530-534, Oct.1993.

[12] W. Chen, A. Q. Huang, C. Li, G. Wang, and W. Gu, "Analysis and Comparison of Medium Voltage High Power dc/dc Converters for off-shore Wind Energy Systems," *IEEE Trans. Power Electron.,* vol. 28, pp.2014-2023, Apr.2013.

[13] A. Averberg and A. Mertens, "Characteristics of the single active bridge converter with voltage doubler," in *Proc. 13th Internatinal Power Electron. And Motion Control Conf.,* 2008.